Solid Freeform Fabrication 2017: Proceedings of the 28th Annual International Solid Freeform Fabrication Symposium – An Additive Manufacturing Conference
Reviewed Paper

Numerical simulation of temperature fields in powder bed fusion process by using hybrid heat source model

Zhibo Luo*, Yaoyao Fiona Zhao*

*Department of Mechanical Engineering, McGill University, Montreal, QC, Canada

Abstract

Powder bed fusion (PBF) process is capable of producing a complex geometrical part with less material and energy consumption compared with conventional manufacturing methods. The performance of PBF processed part is mainly controlled by many process parameters such as scanning speed, scanning pattern, scanning strategy, and layer thickness. Usually, these parameters are optimized through detailed experiments which are time-consuming and costly. Therefore, numerical methods have been widely adopted to investigate the effects of these process parameters on temperature fields and thermal stress fields. As the laser/electron beam introduces huge temperature gradients within the irradiated region, which will result in the distortion even delamination of solidified layers, the study of the history of temperature distribution is the basic and crucial step in the modeling of PBF process. Most of the current research utilizes moving Gaussian point heat source as heat input to model the temperature distribution of a part. However, due to the small diameter of laser/electron beam, a small enough time step size is required to accurately model the real heat input, which will lead to significant computational burden. In this research, a hybrid of moving Gaussian point and line heat source model is developed, which makes the modeling of PBF process efficient without losing too much accuracy. In addition, an adaptive mesh scheme, which is capable of dynamically refining the mesh near the beam spot and coarsening the mesh far away from the beam spot, is adopted to accelerate the simulation process. Specifically, moving Gaussian point heat source is applied to the region of interest where accuracy is more concerned such as the temperature field within overhang feature. While the line heat source is applied to the region of interest where efficiency is more concerned such as temperature field within the inner region of a square. The simulation result shows that the temperature fields by using hybrid source model are comparable to the temperature fields by using the moving Gaussian point heat source model, and much less central processing unit time is required when the hybrid heat source is applied.

1. Introduction

Powder bed fusion (PBF) process, which mainly consists of Selective Laser Melting/Sintering (SLM/SLS) process and Electron Beam Melting (EBM) process, is one of the seven Additive Manufacturing (AM) processes. The high-energy beam is applied by the PBF process to selectively melt the powder with desired shape layer by layer and finally fabricate nearly full density part without too much post-process procedures [1]. PBF process has been widely used in the industry of automobile, aerospace, biomedical, and energy. It has a lot of merits over traditional manufacturing processes [2] such as the ability to fabricate a part with complex geometry features which cannot be manufactured through conventional manufacturing methods; cost effective for single high complexity part or small batches of production; the ability to fabricate an assembled product which results in reduced assembly need. However, several process deficiencies such as balling effect [3, 4], deteriorated surface finish [5], part shrinkage

[6], pores and micro-cracks [7], and residual stress-induced deformation, have been discovered and remain as unsolved issues in PBF process. The high-temperature gradient is the main factor for causing these defects. Especially for a part with overhang features, high-temperature gradient results in the deformation of overhang features and support structures are definitely needed in order to build it successfully. When laser or electron beam rapidly irradiates on the powder bed, the high-temperature gradient will be induced due to the rapid heating of top surface powder layer and slow heat conduction of underlying layers [8, 9]. The development of these high-temperature gradients yields non-homogeneous permanent strains and thermal stresses distribution within solidified layers. In addition, the back-and-forth scanning strategy also results in the repeated expansion and contraction of the adjacent zones. This periodical repetition of thermal expansion and part shrinkage result in the development of residual stress within the solidified layers and geometrical deformation of the end part [10, 11]. Therefore, the development of temperature fields is crucial for the deformation of the final part.

Most of the existing research in the modeling of PBF process utilize the moving Gaussian heat source to simulate the temperature field. And then the obtained temperature field will be used to calculate the thermal stress field during the cooling process and finally get the residual stress when solidified layers are cooled down to the room temperature. Using this method can model the physical process accurately. However, the computational cost will be very high. This is because, for a single scanning track, tens of hundreds of loading steps are needed in order to accurately simulate the real heating process by using moving heat source. In addition, the high-temperature gradient among the melt pool requires the mesh of this area to be very fine. As the scanning speed is very fast, the irradiation time of each point on the scanning track will be very short. If each point can be irradiated and melted at the same time, which means a line Gaussian heat source instead of moving Gaussian heat source is applied to the scanning track, the problem of computational cost can be greatly relieved. This research will try to prove the effectiveness of using line Gaussian heat source model to simulate the temperature field in SLM process. Then, a hybrid heat source which combines the moving Gaussian point heat source and Gaussian line heat source will be put forward to investigate the temperature field of a part being built.

Next, section 2 will review the existing methods in the modeling of PBF process. Section 3 will briefly introduce the numerical model and proposed Gaussian line heat source and hybrid heat source used in this research to predict the temperature distribution. Section 4 will present the verification and simulation results of the proposed new heat sources. The conclusion and future work will be summarized in the last.

2. Literature Review

The development of temperature fields and thermal stress fields in PBF process are greatly dependent on the process parameters such as scanning speed, scanning pattern, scanning strategy, layer thickness, and laser or electron beam related parameters. Usually, these parameters are optimized through detailed experiments which are time-consuming and costly [12, 13]. Therefore, numerical methods are widely applied to investigate the effects of these process parameters on temperature fields and thermal stress fields. Compared with experimental methods, numerical simulations present a whole view of the thermal dynamic and mechanical behavior of the part and the melt pool during the heating and cooling processes.

As the temperature field is the basis for the following mechanical analysis of thermal stress field, different FE models have been developed to estimate the temperature field. A finite

element analysis of temperature field and thermal stress field in PBF needs to consider the following five aspects. 1) Geometry model. Due to the complexity of the real problem, many of the current research only simulate the temperature fields and stress fields in one single track or one layer [14-17]. The shape is usually a simple rectangle or cuboid. For 3D models, 'T' shape and 'L' shape are the widely used geometry model. 2) Finite element mesh model used to represent the geometry model. Hexahedron element has been widely used in most 3D models to represent the printing part and surrounding powders. As the temperature gradient near the melt pool is extremely high, a local refinement mesh or even adaptive mesh should be used during the simulation process [18]. In addition, the adaptive mesh is able to reduce computational time and yield more accurate results compared to the static finite element mesh [19]. 3) Material model used to define the temperature dependent material properties. It is essential to take an effective material model into account when material properties are greatly changed during the heating and cooling processes. It has been concluded that thermal conductivity, specific heat, density, elastic modulus, yield strength, and thermal expansion coefficient are changed significantly when the temperature rise up to the melting point [20]. For example, Tolochko et al. [21] presented that the continuity of thermal conductivity with respect to the temperature is broken at the melting point. In addition, phase change induced latent heat will also have a significant influence on the temperature field. The effect of latent heat on the temperature field is taken into account by defining an equivalent specific heat which increases significantly at the melting point [22]. Though the inclusion of latent heat will increase the accuracy of the simulation results, tons of computational effort is required. 4) Heat source model used to represent the laser energy input. The heat source model is critical to simulate the heat input in the SLM. Some studies model the heat source as a temperature load [23, 24] while most common used heat source is the moving Gaussian heat source [17]. 5) Boundary and initial conditions used to represent the heat loss and initial temperatures. Boundary conditions in the heat transfer of SLM mainly include thermal convection, thermal conduction, and thermal radiation. The heat loss from the bottom of the substrate [25] and surface radiation [16, 26] are usually ignored for the reason of simplification. While some other research [15, 27] include the impact of thermal radiation. Though these simplifications can reduce the accuracy of the results, the loss of accuracy is very small because the main heat transfer mechanism is the conduction through the powder bed and solidified layers [28].

The transient temperature history of powder bed and solidified layers is vital for the determination of the thermal stress distribution and final residual stress. Follow the above-mentioned procedures, many FE models have been developed to estimate the temperature field during PBF process. Fu and Guo [3] develop a 3D-FEM to understand the fundamental temperature gradient mechanism by incorporating layer buildup approach coupled with the moving heat flux in SLM. Ma and Bin [12] propose a model using different scanning patterns in SLS process to estimate the evolution of temperature, thermal stress, and distortion within a single metallic layer. Gusarov et al. [29] propose a numerical model to investigate a single track on a layer of loose powder bed. The results show that the maximum temperature is slightly shifted away from the center of the laser beam. Dai and Shaw [13, 30] propose a finite element method to investigate the influence of fabrication sequence, scanning pattern, and scanning rate on the temperature distribution as well as stress distribution. After the temperature history has been obtained, a transient stress analysis will be executed by changing the analysis type from thermal to structural. The obtained temperature history is applied as a thermal load for the mechanical analysis. Zaeh and Branner [31] present a model to simulate the transient physical

effects and identifies the heat impact on residual stress and deformations through a coupled thermo-mechanical model. Mercelis and Kruth [32] develop a simple theoretical model to predict the residual stress distribution for SLM/SMS process. The theoretical assumptions can be validated through experiments. Vasinonta and Beuth [33] present a thermomechanical model which involving a moving heat source to build thin-walled structures by using laser based solid freeform fabrication process.

3. Numerical modeling

During the laser heating and cooling process, there are three different ways to transfer the heat. The heat conduction is propelled by the temperature difference among the processed material. The heat convection is propelled by the difference between the temperature of the surface of the processed material and the temperature of surroundings. The heat radiation happens when the temperature of processed material is higher than that of the surrounding medium.

3.1 Governing equations for transient thermal analysis

For uniformly and continuum isotropic-material, when the material properties are not dependent on the temperature, the governing equation can be obtained through the principle of conservation of energy,

$$\frac{\partial T}{\partial t} - \frac{\lambda}{\rho c}\left(\frac{\partial^2 T}{\partial x^2} + \frac{\partial^2 T}{\partial y^2} + \frac{\partial^2 T}{\partial z^2}\right) = Q_v \rightarrow \frac{\partial T}{\partial t} - a\Delta T = Q_v \qquad \text{eq. (1)}$$

where λ is the thermal conductivity coefficient, c is the specific heat, ρ is the density, Q_v is the internal heat density of unit volume. $a = \lambda/\rho c$ is the thermal diffusivity.

The initial condition with uniform temperature distribution throughout the powder bed before the irradiation of laser beam at time $t = 0$ can be written as

$$T(x, y, z, 0) = T_0(x, y, z) \quad in\ domain\ \Omega\ for\ t = 0 \qquad \text{eq. (2)}$$

The boundary conditions consist of a prescribed temperature on parts of the boundary and a prescribed heat flux on rest parts of the boundary, which specifies the heat exchange between the boundary surface and surrounding medium.

$$T = T_1 \qquad on\ \Gamma_1 \qquad \text{eq. (3)}$$

$$-\lambda \partial T/\partial n = q_c + q_r \qquad on\ \Gamma_2 \qquad \text{eq. (4)}$$

where $\partial T/\partial n$ is the temperature gradient, T_1 is the prescribed temperature on boundary Γ_1, q_c and q_r is the prescribed heat convection term and the heat radiation term on boundary Γ_2, respectively. The two boundaries Γ_1 and Γ_2 satisfy the relation $\partial\Omega = \Gamma_1 \cup \Gamma_2$.

Using the θ-scheme that discretizes the equation in time, equation (1) can be written as

$$\frac{T^n - T^{n-1}}{\tau_n} - a[(1-\theta)\Delta T^{n-1} + \theta \Delta T^n] = [(1-\theta)Q_v^{n-1} + \theta Q_v^n] \qquad \text{eq. (5)}$$

where $\tau_n = t_n - t_{n-1}$ is the time step size, θ is the parameter controls the time discretization method. $\theta = 0$ generates the explicit Euler time discretization; $\theta = 1$ generates the implicit Euler time discretization; $\theta = 0.5$ generates the Crank-Nicolson time discretization.

Given a time discretization method (in this research $\theta = 0.5$), strong form is discretized in time as shown in equation (5). Then by multiplying, integrating by parts, and applying of boundary conditions, the weak formula for solving this heat transfer problem yields the following linear system

$$(M + a\tau_n\theta A)T^n = MT^{n-1} - a\tau_n(1-\theta)AT^{n-1} + \tau_n[(1-\theta)F^{n-1} + \theta F^n] \qquad \text{eq. (6)}$$

where T^n and F^n is the temperature and integrated heat source vector at time step t_n. M, A, is the assembled mass matrix, Laplace matrix, respectively.

The heat source will be incorporated into the heat source vector. Different heat sources result in different temperature fields. Next, Gaussian point heat source model and Gaussian line heat source model will be discussed in detail as shown in Figure 1, and then a hybrid heat source model which integrates the point heat source and line heat source is proposed.

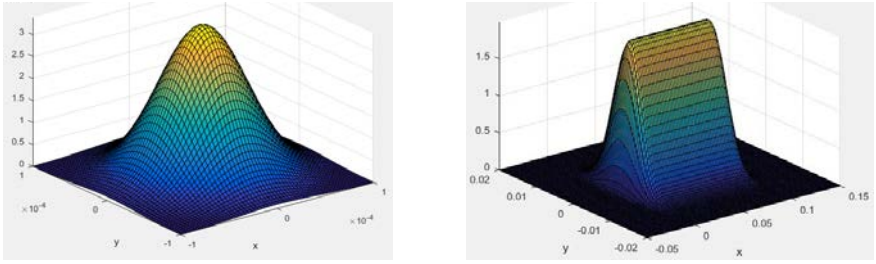

(a) Gaussian point heat source (b) Gaussian line heat source

Figure 1. Categories of Gaussian heat source

3.2 Moving Gaussian point heat source model

When laser or electron beam irradiates on the powder bed, the thermal heat is focused on a very small region. This makes it possible to consider the heat source as Gaussian distributed heat source model, which has been widely applied to analyze the temperature distribution of PBF process. The Gaussian distribution of heat flux can be written as [34]

$$q(r) = q_{max} exp(-Kr^2) \qquad \text{eq. (7)}$$

where q_{max} is the maximum heat flux ($J/mm^2 \cdot s$), K is concentration factor ($1/mm^2$), r is the radial distance of a point to the beam center (mm).

The maximum heat flux can be obtained from the integration of the heat flux over the whole area, which equals to the effective power of the laser beam. With the increase of K, the heat source is more concentrated. Assume that 85% of the heat energy is absorbed within the maximum radius of the laser spot [17], then,

$$q(r) = \frac{2\eta P}{\pi\omega^2} exp\left(-\frac{2r^2}{\omega^2}\right) \qquad \text{eq. (8)}$$

where η is the absorptivity of the powder material, P is the laser power, ω is the maximum radius of the laser spot.

When the laser beam irradiates on the powder bed, most of the thermal heat is absorbed by the powder surface within several microns in depth, which is much smaller compared with the powder and element size. Therefore, the heat source for SLM process can be considered as a surface-based heat source. While the electron beam penetrates the powder bed much deeper as

the electric current can cross over the whole powder. Therefore, the heat source for EBM process can be considered as a volume-based heat source. As the motion of the Gaussian point heat source, the moving Gaussian point heat source (PHS) model for the SLM process and the EBM process can be expressed in the following equations:

For the surface-based heat source,

$$q(x,y,z,t)|_{z=height\ of\ top\ surface} = \frac{2\eta P}{\pi\omega^2} exp\left(-\frac{2[y^2+(x+v\cdot t)^2]}{\omega^2}\right) \qquad \text{eq. (9)}$$

For the volume-based heat source,

$$q(x,y,z,t) = \frac{6\sqrt{3}\eta P}{abc\pi\sqrt{\pi}} exp\left(-\frac{3(x+v\cdot t)^2}{a^2}-\frac{3y^2}{b^2}-\frac{3z^2}{c^2}\right) \qquad \text{eq. (10)}$$

where $a, b,$ and c represents the length of the semi-axis of the Goldak's ellipsoid distribution [34] along $x, y,$ and z directions, respectively.

3.3 Gaussian line heat source model

During PBF process, the scanning speed of the heat source is very fast. Therefore, the moving Gaussian point heat source can be considered as a Gaussian line heat source (LHS), which is displayed in Figure 1, respectively. When the heat source moves along the *x* direction, a or ω is the relevant parameter used to determine the increment of time step. Usually, a is very small and the size of time step should satisfy the relation $\Delta t \le a/v$, otherwise the heat source model will skip over some elements. Therefore, a large number of time steps are required to accurately simulate the continuous motion of the heat source along a line. To overcome this restriction, equation (9) and (10) are averaged over the period of a time step

$$\bar{q}(x,y,z,t) = \frac{1}{\Delta t}\int_{t_0}^{t_0+\Delta t} q(x,y,z,t)dt \qquad \text{eq. (11)}$$

where t_0 is the initial time at the beginning, Δt is the time step. By substituting equation (10) into the above equation, the averaged heat source model or LHS model can be expressed as:

For the surface-based heat source,

$$\bar{q}(x,y,t) = \frac{\eta P}{\Delta t\cdot v\cdot\omega\cdot\sqrt{2\pi}} exp\left(-\frac{2y^2}{\omega^2}\right)\text{erf}\left(\frac{\sqrt{2}(x+vt)}{\omega}\right)|_{t=t_0}^{t_0+\Delta t} \qquad \text{eq. (12)}$$

For the volume-based heat source,

$$\bar{q}(x,y,z,t) = \frac{3\eta P}{\Delta t\cdot v\cdot b\cdot c\cdot\pi} exp\left(-\frac{3y^2}{b^2}-\frac{3z^2}{c^2}\right)\text{erf}\left(\frac{\sqrt{3}(x+vt)}{a}\right)|_{t=t_0}^{t_0+\Delta t} \qquad \text{eq. (13)}$$

This formulation allows time step to be made arbitrarily large without skipping any elements. And it can be noted that as $\Delta t \to 0$, the LHS model becomes the moving Gaussian PHS model.

3.4 Hybrid heat source model

It is easy to know that the LHS will reduce the solution accuracy of final temperature field when modeling the PBF process. To deal with this problem, a hybrid heat source, which

combines the moving Gaussian PHS and the Gaussian LHS, is proposed in this research. Specifically, the moving Gaussian PHS will be applied in the domain where close to the boundaries. While the Gaussian LHS will be applied in the other domain where has similar heat transfer conditions. Then the hybrid heat source (HHS) can be expressed as

$$q = \begin{cases} q_l & p(x,y,z) \in \Omega_l \\ q_p & p(x,y,z) \in \Omega \backslash \Omega_l = \Omega_p \end{cases} \qquad \text{eq. (14)}$$

where q_l represents the Gaussian line heat input, q_p represents the Gaussian point heat input. Ω_l is the domain where LHS should be applied, and Ω_p is the domain where PHS should be applied. $p(x,y,z)$ is a point in the Cartesian coordinates.

4. Verification and simulation results

4.1 Verification

In order to validate the accuracy and deviation as well as the efficiency of the proposed LHS model and HHS model, several simulations are implemented with the same simulation parameters and the results are compared with the result of the moving Gaussian PHS model.

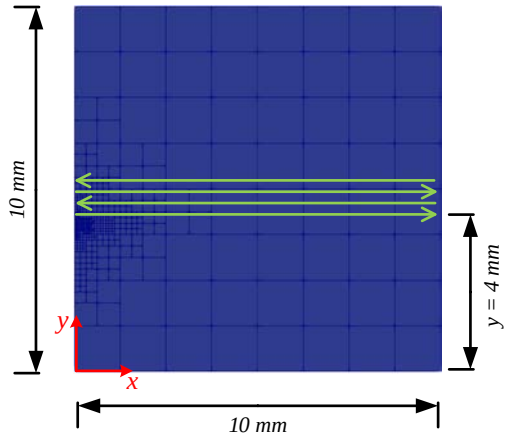

Figure 2. initial 2D finite element mesh for validation

A two-dimensional FEM with adaptive mesh is developed to validate the LHS model and HHS model. The dimension and initial finite element mesh are shown in Figure 2. Specifically, a $10 \times 10\ mm^2$stainless steel substrate is heated by four scanning tracks starting at y = 4 mm with a “S” scanning pattern. The material density is 7900 kg/m^3, thermal conductivity is 20 W/m*K, and specific heat is 480 J/kg*K. The parameters for the laser beam are listed in Table 1. The laser power is P=100 W, the diameter of the laser spot is d = 0.15 mm, the length of each scanning track is 10 mm, and the scanning speed is V=50 mm/s.

Table 1. Simulation parameters of the laser beam

Parameters of the laser beam	Values
Power	100 W
Laser type	Gaussian distribution
Scanning speed	50 mm/s
Scanning pattern	'S' pattern
Absorptivity of the powder	0.7
Printing time for each scanning track	0.2 s
Hatch spacing	75 um
Spot size	150 um

For the thermal model, the boundary condition is to apply a uniform free heat convection of 10 W/m^2*K along all the free surfaces. Both of the ambient temperature and initial temperature of the part model are set to 300 K.

During the simulation, the adaptive mesh scheme with the four-node linear quadratic element is generated and the mesh model is refined and coarsened for each time steps. The simulation is implemented with the open source finite element code named Deal.II [35]. The mesh is initially refined 3 times globally. And the initial time step is implemented for 7 times in order to capture the very small region of the heat input. In order to make sure that the laser spot covers at least 9 elements, the minimum refinement degree (n) should satisfy the following constraint

$$\frac{L}{2^n} \leq \frac{d}{3} \qquad \text{eq. (15)}$$

where L is the length of the part, d is the diameter of the laser spot.

In order to make sure that the moving Gaussian PHS will not skip any element, the maximum time step should satisfy the following constraint

$$\Delta t \leq \frac{d}{V} \qquad \text{eq. (16)}$$

where d is the diameter of the laser spot, V is the scanning speed of the laser beam.

For the LHS model, assume that the length of the line segment is ΔL, then the maximum time step should be:

$$\Delta t \leq \frac{\Delta L}{V} \qquad \text{eq. (17)}$$

Compare equation (16) and equation (17), if $\Delta L \gg d$, i.e. $\Delta L = 10d$, then the step increment can be greatly increased and reduce the computational cost.

4.2 Simulation results

Temperature fields and contours of different heat source models are shown in Figure 3. The heat source is applied along y = 4 mm. Each column presents the temperature fields of a heat source at different time points. Each row presents the temperature fields of different heat source at the same time points. Next, the simulation results are compared at different positions and time points.

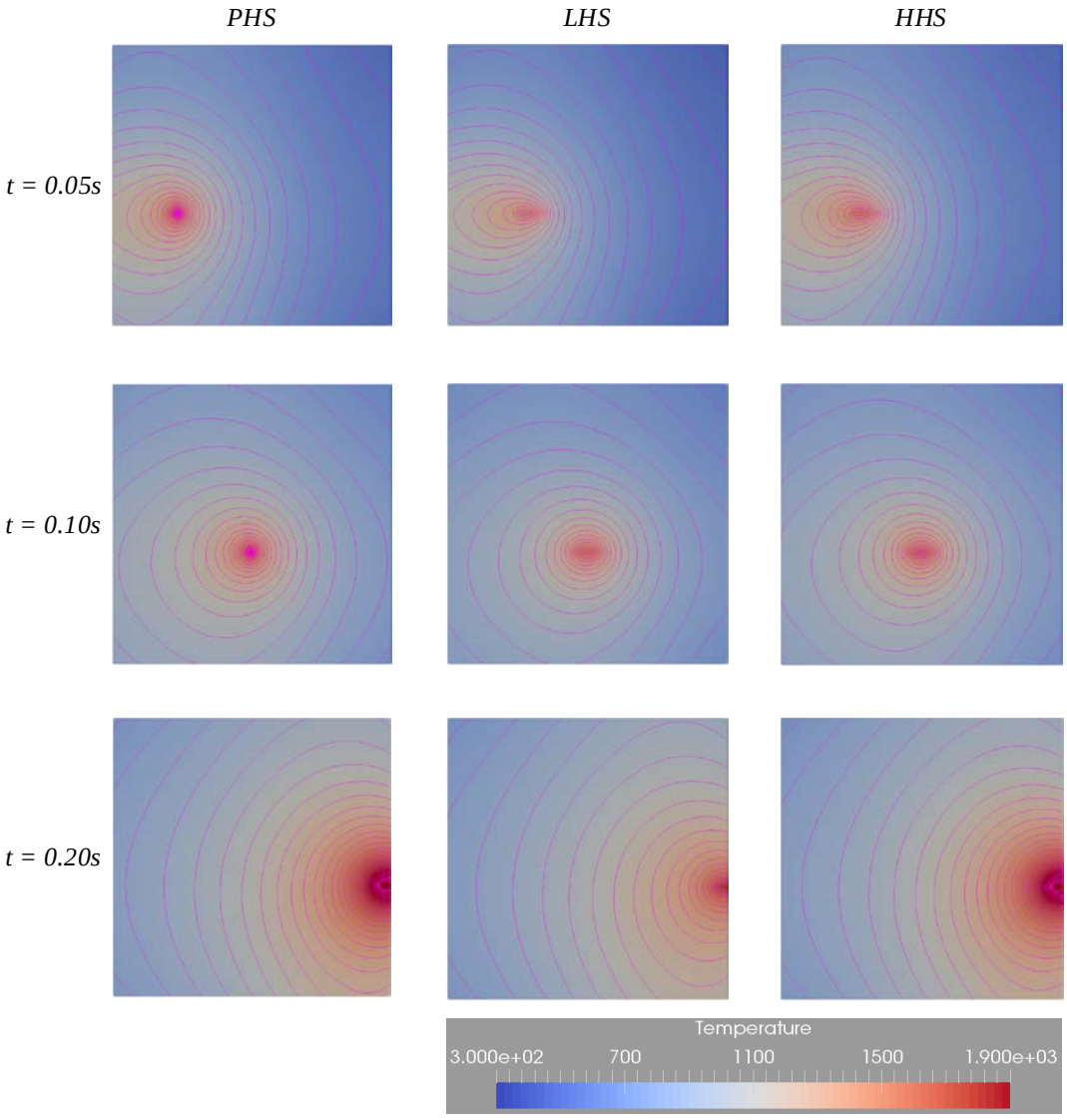

Figure 3. Simulation results of three heat source models at different time points

Simulation times and percent errors of temperature difference for different heat source models are shown in Table 2. The percent errors of temperature difference for thermal results are averaged over the heated scanning track as shown in Figure 4 and are calculated as

$$\epsilon_{temp}(t_n) = \sqrt{\frac{1}{L}\int_{x_0}^{x_0+\Delta x}\left(\frac{T(x_0)-T'(x_0)}{T(x_0)}\right)^2 dx} \times 100\%, t_n = [0, L/V] \qquad \text{eq. (18)}$$

where T and T' are the temperatures obtained from the moving Gaussian PHS and one of the new models (LHS or HHS), respectively. t_n is the time step number. x_0 is the position of the sampling point and $\Delta x = 0.01$ mm. L is the length of single scanning track. $\epsilon_{temp}(t_n)$ is the averaged percent error of temperature difference along a scanning track at time step t_n. Figure 4 illustrates the temperature distributions of different heat source models along the scanning track. For the HHS model, the temperature distribution is quite similar to that of the LHS model when the line heat input is applied. While the temperature distribution is quite similar to that of the moving Gaussian PHS model when the moving point heat input is applied. From Table 2, the temperature difference between the HHS model and the moving Gaussian PHS model is only half of the temperature difference between the LHS model and the moving Gaussian PHS model. In addition, the simulation time of the HHS model and the LHS model decreases to one-third of the moving Gaussian PHS model. This can be attributed to the increased time step size of the HHS model and the LHS model.

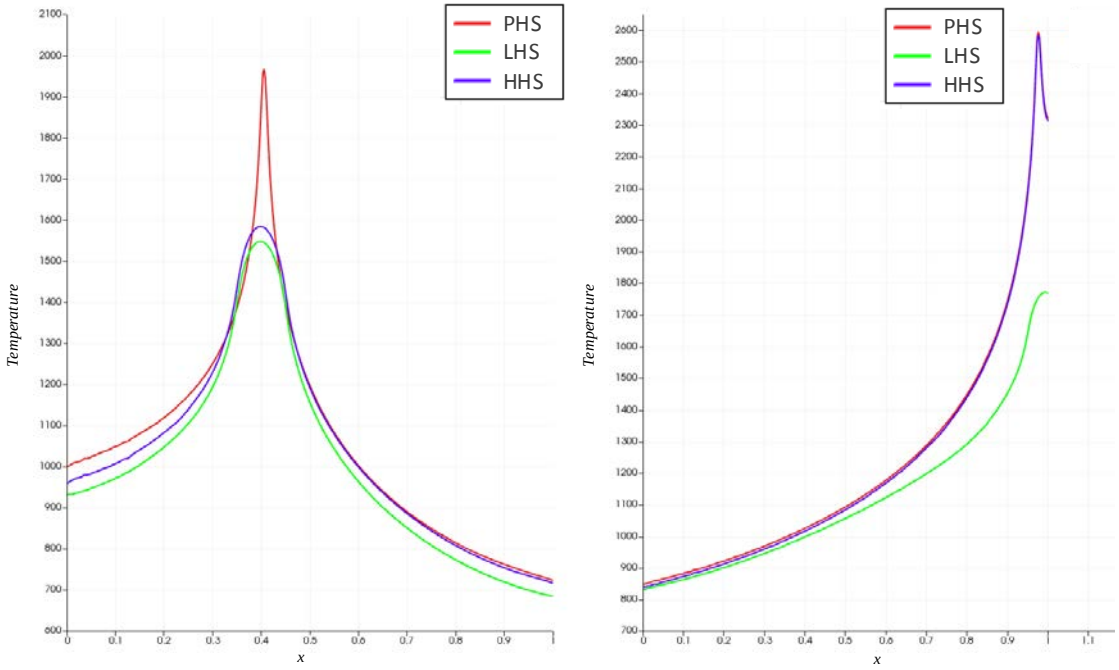

(a) Temperature distributions over y=4 mm at t = 0.084 (s)

(b) Temperature distributions over y=4 mm at t = 0.2 (s)

Figure 4. Temperature distributions of single track for different heat source models at different time points

Table 2. Temperature differences and simulation times for different heat source models

Heat source model	Time increment (s)	Temperature error (%)	Simulation time (s)
Moving PHS (static mesh)	1/500	-	210.6
Moving PHS (adaptive mesh)		< 1	93.7
LHS (10 segments)	1/150	Range = [4.00, 18.43] Average = 7.05	75.2
HHS	1/500 for PHS 1/150 for LHS	Range = [0.69, 9.25] Average = 3.09	100.5/62.6

1. The effect of the scanning speed of the LHS model on the temperature distribution

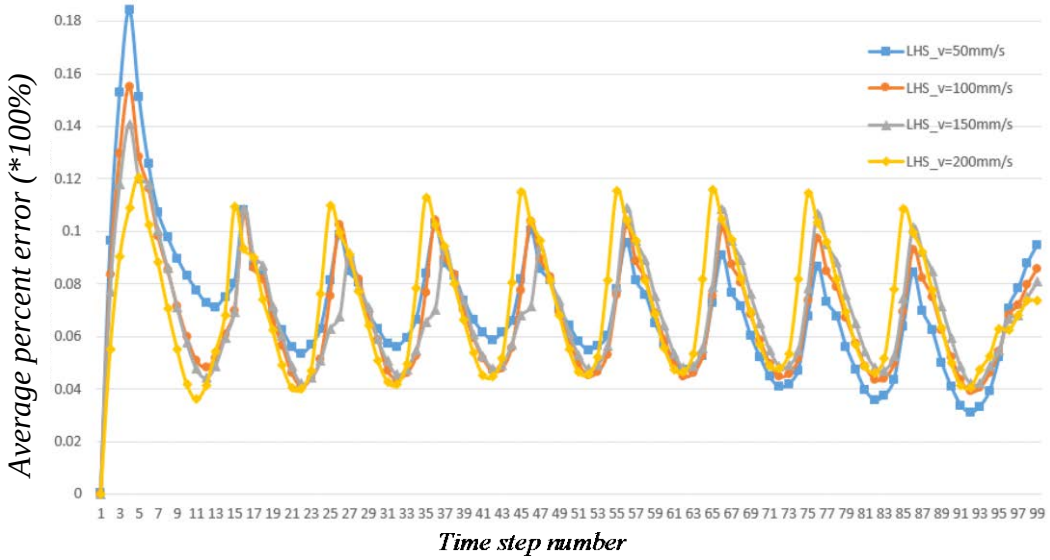

Figure 5. Average percent error of different scanning speed in LHS model

The scanning speed directly determines the size of the time step as shown in equation (16) and (17). Average percent errors of the LHS model along y = 4 mm with different scanning speed are illustrated in Figure 5. The peaks and valleys indicate the beginning and ending of the applied line heat source, respectively. The number of peaks or valleys equals to the number of line segments. There are totally 10 peaks for each scanning speed in Figure 5, therefore, the length of the line segment $\Delta L = 1mm$. It can be noted that with the increase of the scanning speed, the LHS model becomes much stable, which means that the change of the average percent error with the time step exhibits more periodical variation. Though the value of the peak increases a little with the increase of the scanning speed, the value of valley decreases with the increase of the scanning speed. This can be attributed to the fact that less thermal heat is applied

to each line segment as the increase of the scanning speed. Therefore, the maximum temperature value of the LHS decreases with the increase of the scanning speed, which results in the increase of the peak value. In addition, the maximum value of ϵ_{temp} decreases from 18.4% to 12.1% when the scanning speed increases from 50 mm/s to 200 mm/s. While the average value of ϵ_{temp} stays around 7% for each scanning speed. To summarize, for a given LHS model with the same length of the line segment, higher scanning speed exhibits better performance when substituting the moving Gaussian PHS model.

2. The effect of the line segment length of the LHS model on the temperature distribution

It has been proved that the moving Gaussian PHS model can be replaced with the LHS model when the scanning speed is fast enough. In addition, the simulation time can be greatly reduced. However, the length of the LHS cannot be too large because of the solution accuracy. In other words, the time step cannot be too large. In this section, the influence of the line segment length on the temperature distribution of the LHS model will be analyzed in detail.

As shown in equation (11), as the time step $\Delta t \to 0$, the LHS becomes the moving Gaussian PHS. With the increase of the time step, the simulation time decreases while the accuracy decreases as well. Figure 6 illustrates the averaged percent error of temperature difference along y = 4 mm at different time points with different lengths of the line heat source. It can be noted that when the length of line segment $\Delta L = 1mm$, the averaged percent error of each time point sways between 10% and 2%. When the length of line segment $\Delta L = 2mm$, the averaged percent error of each time point sways between 5% and 14%. When the length of the line segment $\Delta L = 0.5mm$, the averaged percent error of each time point decrease to below 5%. The trend of the averaged percent error decreases with the increase of time. This can be attributed to the fact that the applied heat is conducted to the surrounding material uniformly with the increase of time. Considering the efficiency and the accuracy of the simulation, $\Delta L = 1mm$ for the length of the line segment is a good balance.

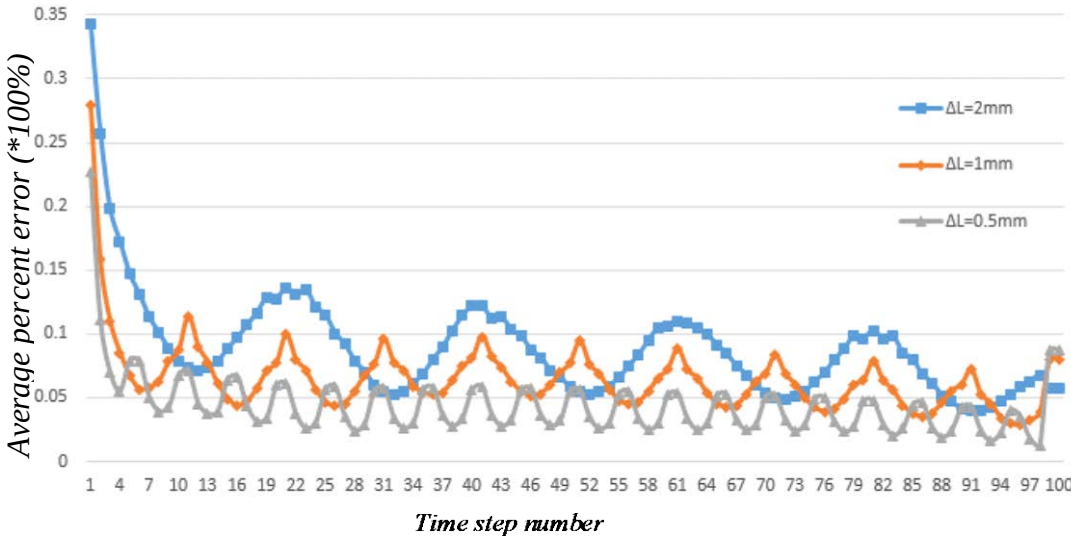

Figure 6. Average percent error of different length of the line segment

3. The effect of the line heat input of the HHS on the temperature distribution

It can be noted that at the beginning and the ending stage of the scanning track as shown in Figure 5 and Figure 6, the temperature difference is quite large. In order to improve the accuracy of the LHS, the moving Gaussian PHS is applied to the crucial regions where temperature gradients are relatively higher than surrounding other regions. For example, the powder material located close to the boundary regions and acute angle regions have different heat transfer conditions. Therefore, the temperature gradient will be different to that of the inner regions, where the temperature gradient is much smooth. This can be shown in Figure 3 and Figure 7. It can be noted that the isothermal lines within the LHS and the moving Gaussian PHS are very similar at the center of the heat source. The difference becomes smaller as the isothermal lines go far away from the heat source. In this section, the influence of the position and the length of the line heat input on the temperature distribution of the HHS model will be discussed.

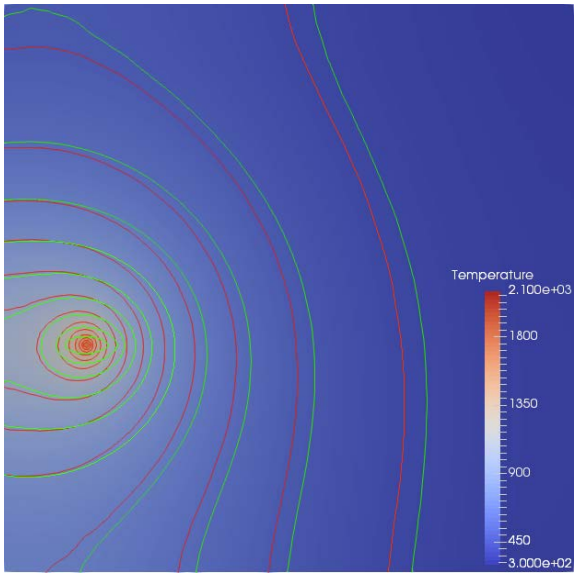

Figure 7. Isothermal lines of the LHS (green lines) and the moving Gaussian PHS (red lines) at time step 15 (t = 0.03 s)

ϵ_{temp} is the averaged percent error of temperature difference between two heat source models over a scanning track at a certain time step. In order to evaluate the averaged percent error over a scanning track for the whole scanning time, ϵ_{temp} is averaged over the whole scanning time of a single track

$$\epsilon_{avg} = \frac{\epsilon_{temp}(t_0)\Delta t + \epsilon_{temp}(t_1)\Delta t + \cdots \epsilon_{temp}(t_n)\Delta t}{t_n - t_0} \times 100\% \qquad \text{eq. (19)}$$

where t_0 and t_n is the start scanning time and the end scanning time of a scanning track, respectively. Δt is the time increment. ϵ_{avg} is the average value of the averaged percent error of a scanning track during a period of the scanning time.

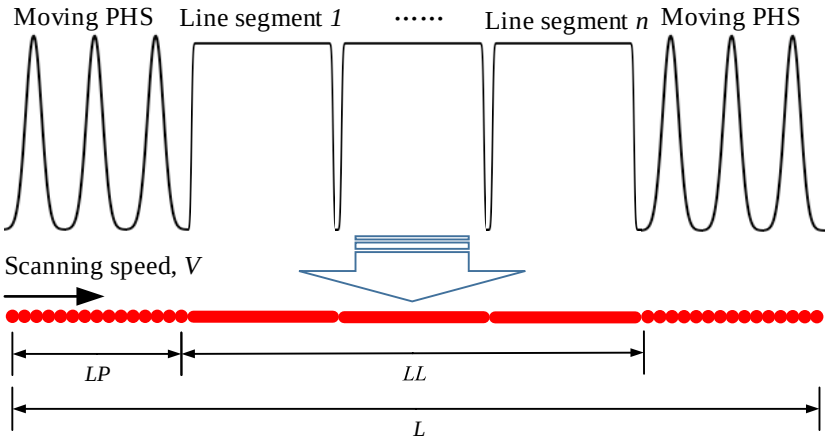

Figure 8. Parameters of the HHS model

As shown in Figure 8, it is assumed that values of the position where line heat source initially applied and the length of the LHS in the HHS are LP and LL, respectively. Error analysis results of four scanning tracks are illustrated in

Figure 9. From

Figure 9, it can be noted that both of the first scanning track of the LHS and the HHS exhibits the largest average temperature difference compared with the moving PHS. And at the beginning and ending stages of the HHS, the average temperature difference is significantly reduced compared with the LHS. Next, several scanning tracks are simulated with different LP and LL in HHS model and the results of ϵ_{avg} are summarized in Figure 10. From Figure 10, it can be noted that the value of ϵ_{avg} first decreases and then increases with the increase of LP; the value of ϵ_{avg} increases with the increase of LL. In addition, the influence of the position where line heat source is applied (LP) on the value of ϵ_{avg} is much smaller compared to that of the total length of line heat source (LL). For this case, when a line heat source with 5 mm length is applied at the exact center of a scanning track with 10 mm, the value of ϵ_{avg} is 3.94%. Therefore, for a square with 10 mm in length and width, the line heat source can be applied at the center of the square with length of 5 mm.

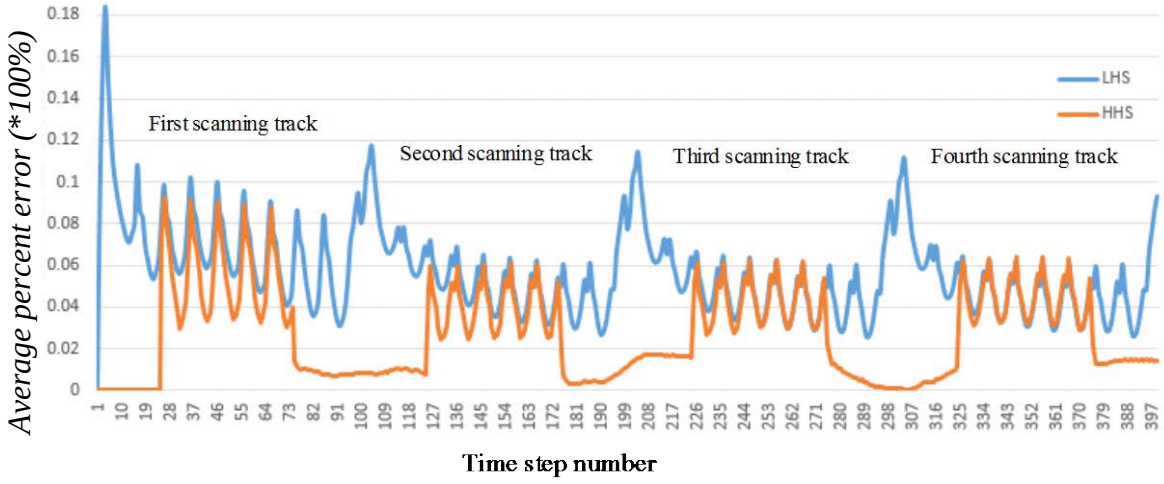

Figure 9. Averaged percent errors of four scanning tracks starting from y = 4 mm

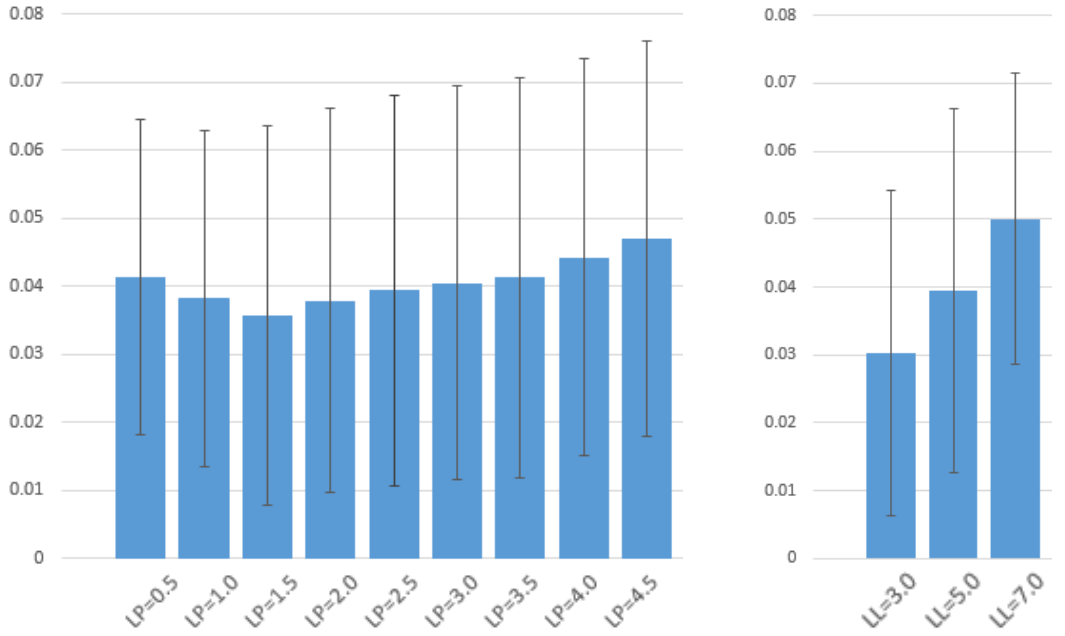

(a) $\mathcal{E}_{avg}$ of different *LP (mm)* (b) $\mathcal{E}_{avg}$ of different *LL (mm)*

Figure 10.Values of ϵ_{avg} with different LP and LL in HHS model

5. Conclusions

This paper proposes a hybrid heat source model, which consists of the LHS and the moving Gaussian PHS, to simulate the temperature field of the PBF process. In addition, adaptive mesh scheme is adopted in this research. Compared with the static mesh scheme, the simulation time of the adaptive mesh scheme is much faster due to the decreased number of elements. The HHS model is able to significantly reduce the simulation time compared to the moving Gaussian PHS model and improve the accuracy of the final temperature distribution compared to the LHS model. The substitution of the moving Gaussian PHS with the LHS leads to around 7% averaged percent error of temperature difference along a scanning track while decreases the simulation time to one-third. While the substitution of the LHS with HHS leads to around 3% averaged percent error of temperature difference along a scanning track. In addition, the HHS model is more effective for the situation where large scanning speed is applied. Therefore, It is more efficient to predict the temperature field of a part being built compared to the implementation of the moving Gaussian PHS model. On the other hand, it is more accurate to predict the temperature field of a part being built compared to the implementation of the LHS model.

From the result of simulation and analysis, it can assume that it is equivalent to apply the HHS instead of the moving Gaussian PHS to simulate the laser scanning of each track if the solution error can be acceptable. Continuous work of this research includes the application of temperature dependent material properties and weak-coupled thermal stress analysis. Furthermore, the LHS model and the HHS model will be implemented in 3D heat transfer process.

References

[1] J.-P. Kruth, L. Froyen, J. Van Vaerenbergh, P. Mercelis, M. Rombouts, and B. Lauwers, "Selective laser melting of iron-based powder," *Journal of Materials Processing Technology,* vol. 149, pp. 616-622, 2004.

[2] J. Slotwinski, "Additive manufacturing: Overview and NDE challenges," in *40TH ANNUAL REVIEW OF PROGRESS IN QUANTITATIVE NONDESTRUCTIVE EVALUATION: Incorporating the 10th International Conference on Barkhausen Noise and Micromagnetic Testing*, 2014, pp. 1173-1177.

[3] C. Fu and Y. Guo, "Three-Dimensional Temperature Gradient Mechanism in Selective Laser Melting of Ti-6Al-4V," *Journal of Manufacturing Science and Engineering,* vol. 136, p. 061004, 2014.

[4] C. Körner, E. Attar, and P. Heinl, "Mesoscopic simulation of selective beam melting processes," *Journal of Materials Processing Technology,* vol. 211, pp. 978-987, 2011.

[5] R. Ippolito, L. Iuliano, and A. Gatto, "Benchmarking of rapid prototyping techniques in terms of dimensional accuracy and surface finish," *CIRP Annals-Manufacturing Technology,* vol. 44, pp. 157-160, 1995.

[6] H. J. Yang, P. J. Hwang, and S. H. Lee, "A study on shrinkage compensation of the SLS process by using the Taguchi method," *International Journal of Machine Tools and Manufacture,* vol. 42, pp. 1203-1212, 9// 2002.

[7] A. Bauereiß, T. Scharowsky, and C. Körner, "Defect generation and propagation mechanism during additive manufacturing by selective beam melting," *Journal of Materials Processing Technology,* 2014.

[8] P. Vora, K. Mumtaz, I. Todd, and N. Hopkinson, "AlSi12 in-situ alloy formation and residual stress reduction using anchorless selective laser melting," *Additive Manufacturing,* vol. 7, pp. 12-19, 2015.

[9] J. P. Kruth, G. Levy, F. Klocke, and T. H. C. Childs, "Consolidation phenomena in laser and powder-bed based layered manufacturing," *CIRP Annals - Manufacturing Technology,* vol. 56, pp. 730-759, // 2007.

[10] M. Shiomi, K. Osakada, K. Nakamura, T. Yamashita, and F. Abe, "Residual Stress within Metallic Model Made by Selective Laser Melting Process," *CIRP Annals - Manufacturing Technology,* vol. 53, pp. 195-198, // 2004.

[11] M. S. A. Aziz, T. Furumoto, T. Ueda, S. Abe, A. Hosokawa, and R. Tanaka, "Study on thermal and strain behaviour in selective laser sintering process," in *Key Engineering Materials* vol. 516, ed, 2012, pp. 203-208.

[12] L. Ma and H. Bin, "Temperature and stress analysis and simulation in fractal scanning-based laser sintering," *The International Journal of Advanced Manufacturing Technology,* vol. 34, pp. 898-903, 2007.

[13] K. Dai and L. Shaw, "Thermal and stress modeling of multi-material laser processing," *Acta Materialia,* vol. 49, pp. 4171-4181, 12/3/ 2001.

[14] I. A. Roberts, "Investigation of residual stresses in the laser melting of metal powders in additive layer manufacturing," University of Wolverhampton West Midlands, 2012.

[15] D. Gu and B. He, "Finite element simulation and experimental investigation of residual stresses in selective laser melted Ti–Ni shape memory alloy," *Computational Materials Science,* vol. 117, pp. 221-232, 5// 2016.

[16] Y. Huang, L. J. Yang, X. Z. Du, and Y. P. Yang, "Finite element analysis of thermal behavior of metal powder during selective laser melting," *International Journal of Thermal Sciences,* vol. 104, pp. 146-157, 6// 2016.

[17] A. Hussein, L. Hao, C. Yan, and R. Everson, "Finite element simulation of the temperature and stress fields in single layers built without-support in selective laser melting," *Materials & Design,* vol. 52, pp. 638-647, 12// 2013.

[18] D. Riedlbauer, P. Steinmann, and J. Mergheim, "Thermomechanical finite element simulations of selective electron beam melting processes: performance considerations," *Computational Mechanics,* vol. 54, pp. 109-122, 2014.

[19] M. J. Berger and J. Oliger, "Adaptive mesh refinement for hyperbolic partial differential equations," *Journal of computational Physics,* vol. 53, pp. 484-512, 1984.

[20] F. Kong and R. Kovacevic, "3D finite element modeling of the thermally induced residual stress in the hybrid laser/arc welding of lap joint," *Journal of Materials Processing Technology,* vol. 210, pp. 941-950, 2010.

[21] N. K. Tolochko, M. K. Arshinov, A. V. Gusarov, V. I. Titov, T. Laoui, and L. Froyen, "Mechanisms of selective laser sintering and heat transfer in Ti powder," *Rapid Prototyping Journal,* vol. 9, pp. 314-326, 2003.

[22] M. Megahed, H.-W. Mindt, N. N'Dri, H. Duan, and O. Desmaison, "Metal additive-manufacturing process and residual stress modeling," *Integrating Materials and Manufacturing Innovation,* vol. 5, pp. 1-33, 2016.

[23] C. Li, C. H. Fu, Y. B. Guo, and F. Z. Fang, "A multiscale modeling approach for fast prediction of part distortion in selective laser melting," *Journal of Materials Processing Technology,* vol. 229, pp. 703-712, 2016.

[24] J. Schilp, C. Seidel, H. Krauss, and J. Weirather, "Investigations on temperature fields during laser beam melting by means of process monitoring and multiscale process modelling," *Advances in Mechanical Engineering,* vol. 6, p. 217584, 2014.

[25] J. Zhang, D. Li, J. Li, and L. Zhao, "Numerical simulation of temperature field in selective laser sintering," in *International Conference on Computer and Computing Technologies in Agriculture*, 2010, pp. 474-479.

[26] I. A. Roberts, C. J. Wang, R. Esterlein, M. Stanford, and D. J. Mynors, "A three-dimensional finite element analysis of the temperature field during laser melting of metal powders in additive layer manufacturing," *International Journal of Machine Tools and Manufacture,* vol. 49, pp. 916-923, 10// 2009.

[27] B. Cheng, S. Shrestha, and K. Chou, "Stress and deformation evaluations of scanning strategy effect in selective laser melting," *Additive Manufacturing,* 2016.

[28] B. Schoinochoritis, D. Chantzis, and K. Salonitis, "Simulation of metallic powder bed additive manufacturing processes with the finite element method: A critical review," *Proceedings of the Institution of Mechanical Engineers, Part B: Journal of Engineering Manufacture,* p. 0954405414567522, 2015.

[29] A. Gusarov, I. Yadroitsev, P. Bertrand, and I. Smurov, "Heat transfer modelling and stability analysis of selective laser melting," *Applied Surface Science,* vol. 254, pp. 975-979, 2007.

[30] K. Dai and L. Shaw, "Distortion minimization of laser-processed components through control of laser scanning patterns," *Rapid Prototyping Journal,* vol. 8, pp. 270-276, 2002.

[31] M. F. Zaeh and G. Branner, "Investigations on residual stresses and deformations in selective laser melting," *Production Engineering,* vol. 4, pp. 35-45, 2010.

[32] P. Mercelis and J.-P. Kruth, "Residual stresses in selective laser sintering and selective laser melting," *Rapid Prototyping Journal,* vol. 12, pp. 254-265, 2006.

[33] A. Vasinonta, J. Beuth, and M. Griffith, "Process maps for controlling residual stress and melt pool size in laser-based SFF processes," in *Solid Freeform Fabrication Proceedings,* 2000, pp. 200-208.

[34] J. Goldak, A. Chakravarti, and M. Bibby, "A new finite element model for welding heat sources," *Metallurgical transactions B,* vol. 15, pp. 299-305, 1984.

[35] W. Bangerth, R. Hartmann, and G. Kanschat, "deal. II—a general-purpose object-oriented finite element library," *ACM Transactions on Mathematical Software (TOMS),* vol. 33, p. 24, 2007.